Field-Dependent Domain Distortion and Interlayer Polarization Distribution in PbTiO₃/SrTiO₃ Superlattices

Pice Chen,[1] Margaret P. Cosgriff,[1] Qingteng Zhang,[1] Sara J. Callori,[2] Bernhard W. Adams,[3]
Eric M. Dufresne,[3] Matthew Dawber,[2] and Paul G. Evans[1,*]

[1]*Department of Materials Science and Engineering & Materials Science Program, University of Wisconsin-Madison,
Madison, Wisconsin 53706, USA*
[2]*Department of Physics and Astronomy, Stony Brook University, Stony Brook, New York 11794, USA*
[3]*Advanced Photon Source, Argonne National Laboratory, Argonne, Illinois 60439, USA*

The remnant polarization of weakly coupled ferroelectric-dielectric superlattices is distributed unequally between the component layers, and as a result the components respond differently to applied electric fields. The difference is apparent in both the nanometer-scale structure of striped polarization domains and in the development of piezoelectric strain and field-induced polarization. Both effects are probed with *in situ* time-resolved synchrotron x-ray diffraction in a PbTiO₃/SrTiO₃ superlattice in fields up to 2.38 MV/cm. Domains are initially distorted to increase the polarization in the SrTiO₃ layer while retaining the striped motif. The subsequent transformation to a uniform polarization state at a later time leads to piezoelectric expansion dominated by the field-induced polarization of the SrTiO₃ layers. The results are consistent with theoretical predictions of the field dependence of the domain structure and electrical polarization.

Ferroelectric-dielectric superlattices (SLs) present the opportunity to create novel nanoscale domain configurations of the ferroelectric remnant polarization [1,2]. Electrical and structural properties and the configuration of polarization domains depend in detail on the coupling of the electrical polarization and structural distortion between the component layers of the SLs [3,4]. When the dielectric component is relatively weakly polarized the SLs exhibit a striped nanodomain configuration that is geometrically similar to what is found in ultrathin ferroelectrics [5–7]. The unequal distribution of the polarization between ferroelectric and dielectric components, however, leads to the formation of complex nanoscale variations on the basic striped motif, including vortices at the corners of domains [8]. Applied electric fields result in a transformation to a uniform polarization state in which domains are no longer present [9,10]. The evolution of the polarization-domain configuration and of the atomic structure within each component layer as a function of time during the application of the electric field are not yet known, but would provide insight into the mechanism of the transformation. We show here that the SLs exhibit a series of responses to the applied electric field. First, before the transformation to the uniform polarization state, the field induces a structural distortion of the striped domain pattern that is consistent with an increase of the average polarization within the dielectric layers. Following the disappearance of the domains, the dielectric layers show a large piezoelectric distortion in comparison with the ferroelectric layers. This distribution of the overall piezoelectricity is consistent with the

increase in polarization of the dielectric layers due to the transformation.

The evolution of the structure of the SL following the onset of the applied electric field is conceptually divided into two regimes. In the first regime, which persists for durations of 1 to 100 ns after the onset of the field, the striped domain geometry is metastable [10]. The continued existence of the striped domain pattern leads to mechanical clamping between adjacent domains of opposite polarization, which limits the piezoelectric expansion [10,11]. First-principles calculations predict that, within this clamped structure, the dielectric layers will exhibit domain wall motion and the uniform polarization state can form in the dielectric layers before the ferroelectric layers [12]. The nanosecond time scale of the transformation to the uniform polarization state, however, has made experimental tests of these predictions difficult. In the second regime, the SL switches in some areas into a uniform polarization state while other areas remain in the metastable striped domains [10]. The consequences of the transformation to a uniform polarization state are that the polarization of the dielectric layers must increase to match the ferroelectric layers, and that the dielectric layers must exhibit a piezoelectric expansion commensurate with their polarization. These properties of the uniform polarization state have been predicted for PbTiO₃/SrTiO₃ (PTO/STO) SLs [13], but have not yet been tested experimentally.

In this Letter, we report the atomic scale and domain structure of a PTO/STO SL in these two regimes of its response to an applied electric field. *In situ* time-resolved synchrotron x-ray microdiffraction was used to probe the

intensities of x-ray reflections arising (i) from the domain pattern and (ii) from the atomic structure of the SL. In the first time regime, the change in the intensities of the domain reflections is consistent with models in which the average polarization of the dielectric STO layers increases. In the second time regime, analysis of the change in the intensities of the SL structural reflections in the applied field shows that the dielectric STO layers exhibit a piezoelectric effect commensurate with the polarization expected due to the elimination of the striped domains.

A PTO/STO SL with a repeating unit of 8 unit cells of PTO and 3 unit cells of STO and an overall thickness of 100 nm was grown on a $SrRuO_3$ bottom electrode on an STO substrate using off-axis radio frequency magnetron sputtering [14]. Capacitors were formed by creating Au thin film top electrodes with diameters of 50 and 130 μm. Time resolved x-ray microdiffraction experiments were conducted at station 7ID-B of the Advanced Photon Source of Argonne National Laboratory [10]. Electric fields were applied along the thickness direction of the SL using a tungsten probe tip in contact with the top electrode. The effective time resolution of the experiment was set by the 85 ns charging time constant of the 50 μm capacitors.

The atomic periodicity of the SL produces x-ray reflections at out-of-plane wave vectors $Q_z = \frac{2\pi}{d_{avg}}(m + \frac{l}{n})$, where the integer m indexes the reflections from the average lattice constant of each unit cell d_{avg}, n is the number of atomic layers in the repeating unit, and l indexes the out-of-plane superlattice satellite reflections. The striped domain pattern [Fig. 1(a)] produces diffuse scattering satellites at the same Q_z as the SL structural reflections, but with nonzero in-plane wave vectors Q_x and Q_y. The striped domain pattern has no preferred in-plane direction, which results in rings of intensity in reciprocal space, as shown in the inset of Fig. 1(b). The intensity in a slice at $Q_x = 0$ through reflections at $m = 2$, i.e., at values of Q_z slightly less than the STO substrate 002 reflection, is shown in Fig. 1(b). The striped domain pattern has intensity maxima at $Q_y = \pm 0.095$ Å^{-1}, corresponding to a domain period of 6.6 nm. The data in Figs. 1 and 3 were acquired using 50 μm-diameter capacitors.

The intensities of the domain satellites depend on the nanoscale distribution of polarization in the domains. These intensities are modified by applied electric fields. Domain satellites near structural reflections at $m = 2$, $l = 0$ and $m = 2$, $l = -1$ at zero field (E off) and at 5 ns during the rising slope of a 2.12 MV/cm electric field (E on) are shown in Fig. 1(c). The intensities of both sets of satellites decrease in the applied field because of the gradual transformation of the SL into the uniform polarization state. The domain satellites disappear in electric fields of either sign, i.e., either parallel or antiparallel to the surface normal. The electric field in the following experiments favored polarization-down domains.
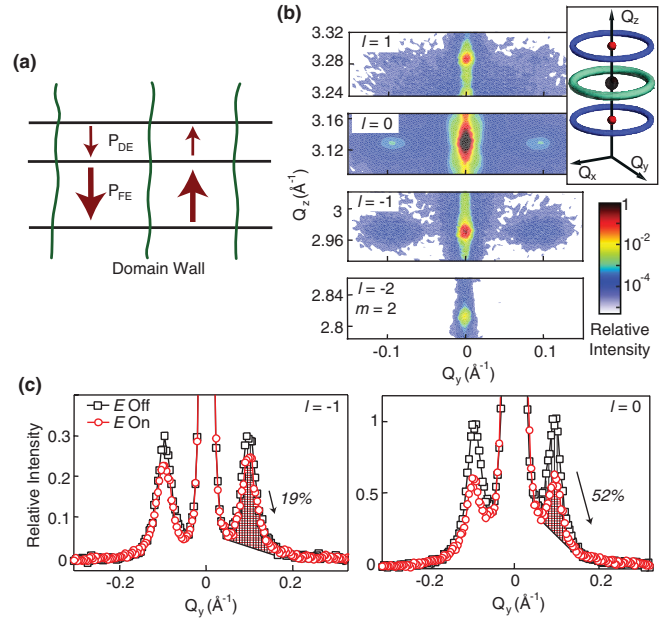

FIG. 1 (color).   (a) Schematic cross section of the striped polarization domain pattern in a weakly coupled ferroelectric-dielectric SL. The formation of domains is driven by the relatively small polarization P_{DE} of the dielectric layers relative to the polarization of the ferroelectric layers P_{FE}. (b) A planar section of reciprocal space at $Q_x = 0$, acquired near the $m = 2$ reflections of the PTO/STO SL. A schematic of the three-dimensional reciprocal space of the SL is shown as an inset. The spheres along $Q_x = Q_y = 0$ and the surrounding rings represent the SL structural reflections and the domain satellite reflections, respectively. (c) Intensity as a function of Q_y for the $m = 2$ and $l = -1$ (left panel) and $l = 0$ (right panel) domain satellites, at zero electric field (squares) and at 5 ns during the rising slope of a 60 ns-duration, 2.12 MV/cm electric field (circles). The shading indicates the areas over which the intensities of the domain satellites are integrated. Intensities in both panels are normalized to the zero-field intensity of the $l = 0$ satellite.

The relative change of the intensities of the domain satellites as a function of the applied field provides insight into the evolution of the structure of the domains. It is immediately apparent that the structure in the applied fields differs from the zero-field structure because the rate at which the intensities of the domain satellites decrease depends on the indices of the reflections. In Fig. 1(c), the field-on intensity of the $l = -1$ domain satellite is 19% lower than the field-off intensity, while the $l = 0$ domain satellite has exhibited a larger decrease of 52%.

The field-induced changes in the relative intensities of the domain satellites can be interpreted using a kinematic x-ray diffraction simulation. The striped domain pattern is included in the simulation by extending the lateral boundaries of the simulated atomic arrangement to encompass a domain period of 16 unit cells. The zero-field simulation applies the STO bulk lattice constant to the STO layers and stretches PTO layers so that the

average lattice constant agrees with the experiment. The PTO fractional atomic positions are chosen to match PTO ceramics [15]. The STO atomic positions are based on theoretical predictions that the polarization in STO layers is 30%–50% of PTO polarization [8,16]. We thus use fractional atomic displacements in STO that are 40% of those in PTO layers. The key results of the simulation do not depend on the magnitude of the initial atomic displacements in STO layers.

We now test the hypothesis that the experimentally observed changes of the intensities of the domain satellites are caused by the modification of the domain configuration within the STO layers. Lisenkov *et al.* predict that the weakly polarized dielectric layers are less stable than the ferroelectric layers under applied electric fields, and consequently that the dielectric layers exhibit increased polarization before the ferroelectric layers [12]. We consider two models to simulate the increased polarization in STO: (i) domain walls in STO are displaced by the field or (ii) atomic positions in the STO layers change in the field. For both models, the electric field changes the average polarization of the STO, but leaves the PTO layer unaffected.

In the first model, domain walls in STO are displaced into the polarization-up domains so that the STO layers develop a net polarization aligned with the field. Situations with zero displacement of the domain walls and with a displacement of two unit cells are shown in Fig. 2(a). We define a quantity R to be the ratio of the intensity of the $m = 2$, $l = -1$ domain satellite to the intensity of the $m = 2$, $l = 0$ domain satellite. The simulation shows, in Fig. 2(b), that the ratio R increases monotonically as the displacement of domain walls in the STO layers increases. In the extreme case where the domain walls are displaced by four unit cells, the stripe domain pattern no longer persists in the STO layers and the ratio R increases by a factor of 2.4. In the second model, we increase the overall polarization of STO layers by reducing the fractional atomic displacements within the polarization-up domains of the STO layers. The simulated ratio R increases, up to 1.6 for the limiting centrosymmetric case, as the fractional atomic displacement is reduced, as shown in Fig. 2(c). Despite their difference in detail, both models show that an increase of the average polarization in STO layers increases R.

The experimentally observed ratio R of domain satellite intensities increases in applied electric fields. Figure 3 shows two sets of measurements of the intensities of domain satellites made during the initial 20 ns of the applied electric fields. The difference between Figs. 3(a) and 3(b) is that the ratio is measured using different segments of the diffuse scattering rings. The increase in R agrees with the kinematical diffraction simulation, and its magnitude is within the range predicted by the models. The essential result is that the domain structure responds to the applied field with a distortion that increases the
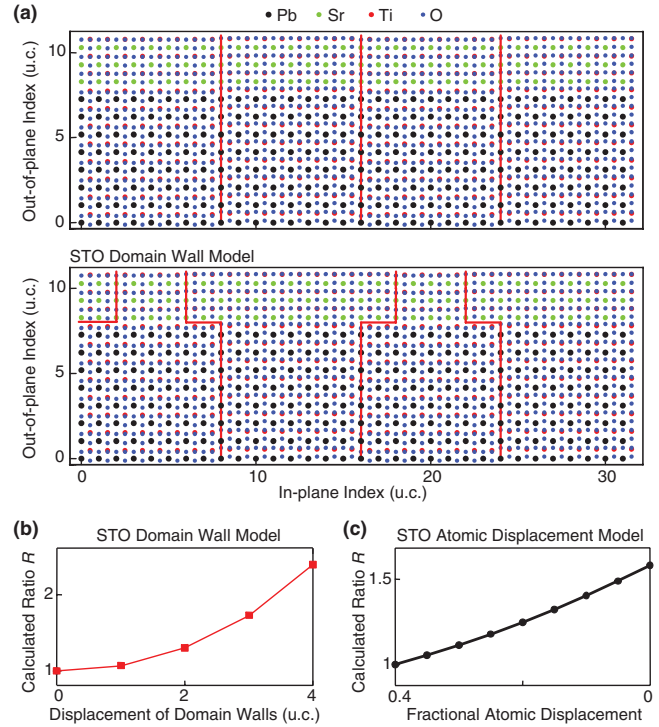

FIG. 2 (color). (a) Atomic positions for the kinematic x-ray scattering simulation, in the cases where the domain walls are vertical (top panel) and displaced by two unit cells toward the polarization-up domains in STO layers (bottom panel). (b) Simulated variation of the change in relative intensities of the domain diffuse scattering satellites as a function of the displacement of domain walls within the STO layers expanding the polarization down configuration. The displacement is given in unit cells (u.c.). R is defined as the ratio of the intensity of the $m = 2$, $l = -1$ domain satellite to the $m = 2$, $l = 0$ domain satellite, normalized to the zero-field value. (c) Simulated change in R resulting from decreased fractional atomic displacement in the polarization-up domains of the STO layers. The fractional atomic displacement is normalized to the value in PTO bulk ceramics.

polarization in the STO layers but not in the PTO layers. The ratio R is time dependent in Fig. 3 because the elapsed time is less than the charging time constant and the magnitude of the field is increasing.

At later times, the domain pattern disappears and only the structural SL x-ray reflections at $Q_x = Q_y = 0$ remain. The intensities of the SL reflections depend on the distribution of piezoelectric distortion between the component layers. Figure 4(a) shows diffraction patterns acquired from 130 μm-diameter capacitors at $E = 0$ and for $E = 2.12$ MV/cm in the uniform polarization state at a time long after the onset of the field. Reflections shift to lower Q_z due to piezoelectric expansion because the clamping is alleviated. And intensities change due to the change in the atomic structure within the repeating unit of the SL. The integrated intensities of several reflections are plotted as a
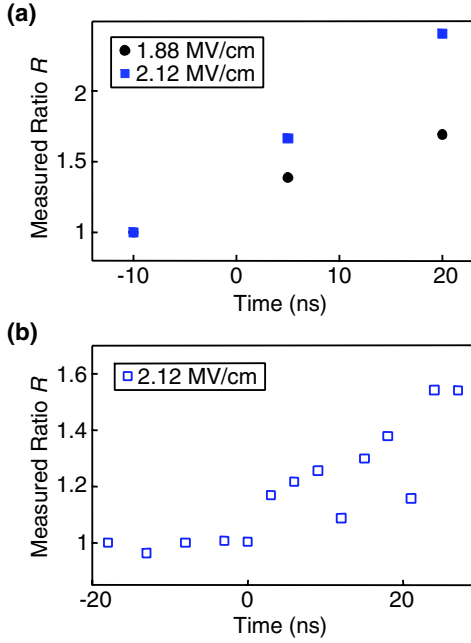
FIG. 3 (color online).   Experimental values of the ratio R of domain satellite intensities, normalized to zero-field values. (a) Measurements based on diffraction patterns separately optimized for the $l = 0$ and $l = -1$ domain satellites. (b) Measurements based on diffraction patterns optimized for $l = 0$ domain satellites that capture a segment of $l = -1$ domain satellites.
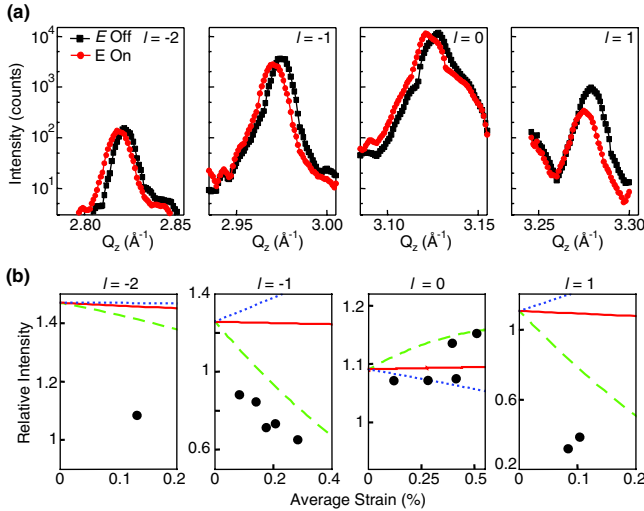

FIG. 4 (color online).   (a) Diffraction patterns of the SL structural reflections with indices $m = 2$ and $l = -2, -1, 0$ and 1 at zero field (squares) and just before the end of a 300 ns-duration electric field with a magnitude of 2.12 MV/cm (circles). The shift of each reflection to a lower wave vector is due to piezoelectric expansion. (b) Integrated intensities of the SL structural reflections with indices $m = 2$ and $l = -2, -1, 0$, and 1 as a function of the average strain. The lines are kinematic simulations in which the piezoelectric distortion is equal in PTO and STO layers (solid lines), only in PTO layers (dotted lines), and only in STO layers (dashed lines).

function of the piezoelectric strain in Fig. 4(b), acquired from both 50 and 130 μm-diameter capacitors. The $l = -2$ and $l = 0$ reflections become more intense after the transformation to the uniform-polarization state while the $l = -1$ and $l = 1$ SL reflections decrease in intensity.

A comparison of the experimental results with the kinematic diffraction simulation shows how the PTO and STO layers share the piezoelectric strain. We consider three cases: (i) the distortion is distributed evenly between PTO and STO layers, (ii) the distortion occurs only in PTO layers, and (iii) the distortion occurs only in STO layers. We also include the change of lattice constants due to the piezoelectric expansion and allow the atomic displacements in STO layers to increase as the size of STO unit cells increases. The polarization transformation itself changes the intensities of the SL x-ray reflections. The polarization-down configuration produces x-ray reflections with larger intensities than the zero-field striped domain pattern. A similar dependence of the intensity on the crystallographic direction of the remnant polarization is observed in compositionally uniform $Pb(Zr, Ti)O_3$ thin films [17,18].

The experimentally observed variation of the intensity as a function of the piezoelectric strain is best fit by the case where all of the piezoelectric distortion occurs in the STO layers. The predicted intensities of the $l = -1$ and 1 SL reflections, for example, decrease as the piezoelectric distortion increases, as shown by the dashed lines in Fig. 4(b). The intensity variation in the SL structural reflections shows that the STO layers expand more than PTO layers in the applied electric fields. The larger piezoelectric distortion in STO layers matches the expectation that the field increases the initially small polarization of STO and produces a correspondingly large increase in the piezoelectric expansion [13]. In comparison, $BaTiO_3/CaTiO_3(BTO/CTO)$ SLs are strongly coupled and thus behave as a uniform-polarization ferroelectric with equal expansion in both components [19,20].

We have shown that the relatively weak polarization of the STO layers in a PTO/STO SL has important effects on the evolution of the domain and atomic structure in applied electric fields. The layer-dependent evolution of the nanometer-scale polarization configuration and the associated structural distortion are both consistent with theoretical predictions that applied fields lead to large increases in the polarization of the STO component. X-ray characterization methods provide the atomic-to-nanoscale structural resolution required to understand the dynamic properties of this system. The methods themselves can be extended into other challenges, including the interfacial coupling of improper ferroelectric SLs [4], and the interfacial competition of ferroelectricity and antiferrodistortive order in PTO/STO and BTO/CTO SLs [13,21,22]. Insight into the origin of the time-domain properties of SLs has the potential to increase the functionalities of complex oxides by

providing the means to tune the field and time dependence of electronic properties.

---

*evans@engr.wisc.edu

[1] Y. L. Li et al., Appl. Phys. Lett. **91**, 112914 (2007).

[2] S. Lisenkov and L. Bellaiche, Phys. Rev. B **76**, 020102 (2007).

[3] S. M. Nakhmanson, K. M. Rabe, and D. Vanderbilt, Appl. Phys. Lett. **87**, 102906 (2005).

[4] E. Bousquet, M. Dawber, N. Stucki, C. Lichtensteiger, P. Hermet, S. Gariglio, J. M. Triscone, and P. Ghosez, Nature (London) **452**, 732 (2008).

[5] V. A. Stephanovich, I. A. Luk'yanchuk, and M. G. Karkut, Phys. Rev. Lett. **94**, 047601 (2005).

[6] A. Torres-Pardo, A. Gloter, P. Zubko, N. Jecklin, C. Lichtensteiger, C. Colliex, J.-M. Triscone, and O. Stéphan, Phys. Rev. B **84**, 220102 (2011).

[7] D. D. Fong, G. B. Stephenson, S. K. Streiffer, J. A. Eastman, O. Auciello, P. H. Fuoss, and C. Thompson, Science **304**, 1650 (2004).

[8] P. Aguado-Puente and J. Junquera, Phys. Rev. B **85**, 184105 (2012).

[9] P. Zubko, N. Stucki, C. Lichtensteiger, and J. M. Triscone, Phys. Rev. Lett. **104**, 187601 (2010).

[10] J. Y. Jo, P. Chen, R. J. Sichel, S. J. Callori, J. Sinsheimer, E. M. Dufresne, M. Dawber, and P. G. Evans, Phys. Rev. Lett. **107**, 055501 (2011).

[11] L. Chen and A. L. Roytburd, Appl. Phys. Lett. **90**, 102903 (2007).

[12] S. Lisenkov, I. Ponomareva, and L. Bellaiche, Phys. Rev. B **79**, 024101 (2009).

[13] C. Swartz and X. Wu, Phys. Rev. B **85**, 054102 (2012).

[14] M. Dawber, N. Stucki, C. Lichtensteiger, S. Gariglio, P. Ghosez, and J. M. Triscone, Adv. Mater. **19**, 4153 (2007).

[15] P. P. Neves, A. C. Doriguetto, V. R. Mastelaro, L. P. Lopes, Y. P. Mascarenhas, A. Michalowicz, and J. A. Eiras, J. Phys. Chem. B **108**, 14840 (2004).

[16] D. C. Ma, Y. Zheng, and C. H. Woo, Acta Mater. **57**, 4736 (2009).

[17] D. H. Do, P. G. Evans, E. D. Isaacs, D. M. Kim, C. B. Eom, and E. M. Dufresne, Nat. Mater. **3**, 365 (2004).

[18] J. Y. Jo et al., Nano Lett. **11**, 3080 (2011).

[19] J. Y. Jo, R. J. Sichel, H. N. Lee, S. M. Nakhmanson, E. M. Dufresne, and P. G. Evans, Phys. Rev. Lett. **104**, 207601 (2010).

[20] J. Y. Jo, R. J. Sichel, E. M. Dufresne, H. N. Lee, S. M. Nakhmanson, and P. G. Evans, Phys. Rev. B **82**, 174116 (2010).

[21] X. F. Wu, K. M. Rabe, and D. Vanderbilt, Phys. Rev. B **83**, 020104 (2011).

[22] J. Hong and D. Vanderbilt, arXiv:1212.0608.